Available online at www.sciencedirect.com
ScienceDirect
Journal of Computational Physics 225 (2007) 1020–1038
JOURNAL OF COMPUTATIONAL PHYSICS
www.elsevier.com/locate/jcp

A stable high-order finite difference scheme for the compressible Navier–Stokes equations, far-field boundary conditions

Magnus Svärd [a,*], Mark H. Carpenter [b], Jan Nordström [c,d,e]

[a] Center for Turbulence Research, Building 500, Stanford University, Stanford, CA 94305-3035, USA
[b] Computational Methods and Simulation Branch, NASA Langley Research Center, Hampton, VA 23681-2199, USA
[c] Computational Physics Department, Division of Systems Technology, The Swedish Defence Research Agency, SE-164 90 Stockholm, Sweden
[d] Department of Information Technology, Uppsala University, SE-751 05 Uppsala, Sweden
[e] Dept of Aeronautical and Vehicle Engineering, KTH-The Royal Institute of Technology, SE-100 44 Stockholm, Sweden

Received 26 May 2006; received in revised form 5 December 2006; accepted 12 January 2007
Available online 3 February 2007

Abstract

We construct a stable high-order finite difference scheme for the compressible Navier–Stokes equations, that satisfy an energy estimate. The equations are discretized with high-order accurate finite difference methods that satisfy a Summation-By-Parts rule. The boundary conditions are imposed with penalty terms known as the Simultaneous Approximation Term technique. The main result is a stability proof for the full three-dimensional Navier–Stokes equations, including the boundary conditions.

We show the theoretical third-, fourth-, and fifth-order convergence rate, for a viscous shock, where the analytic solution is known. We demonstrate the stability and discuss the non-reflecting properties of the outflow conditions for a vortex in free space. Furthermore, we compute the three-dimensional vortex shedding behind a circular cylinder in an oblique free stream for Mach number 0.5 and Reynolds number 500.

Keywords: High-order finite difference methods; Boundary conditions; Compressible Navier–Stokes equations; Stability; Accuracy; Well-posedness; Summation-by-Parts; Simultaneous approximation terms

1. Introduction

Solving the Navier–Stokes equations require vast computer resources for realistic applications. Low-order methods are the most commonly used for production calculations. However, it is well known that for simpler problems high-order methods (order $\geqslant 3$) are superior to low-order methods in the sense that a given accuracy can be achieved with much less computer power. (See [1].) The same superiority of high-order methods has been difficult to show for realistic applications.

* Corresponding author. Tel.: +1 650 725 6635.
E-mail address: magnus.svard@gmail.com (M. Svärd).

0021-9991/$ - see front matter © 2007 Elsevier Inc. All rights reserved.
doi:10.1016/j.jcp.2007.01.023

Much of the problems high-order methods have encountered, relate to boundary closures and imposition of boundary conditions, which often introduce instabilities. For low-order methods, fewer numerical boundary conditions are needed and they can often be chosen in an intuitive manner without destroying stability.

With this work we describe a scheme that we believe can extend the usefulness of high-order methods to realistic applications. We will focus on a stable treatment of the far-field boundaries and postpone the discussion of no-slip wall conditions and grid-block interfaces to future articles.

The first step in order to device a stable numerical method is to analyze the well-posedness of the mathematical problem. For smooth solutions to non-linear problems, linear well-posedness implies that small perturbations will not grow and the non-linear problem is therefore well-posed. Assuming existence and uniqueness of solutions, the remaining question is boundedness of the solution, which mainly relates to the boundary conditions.

The boundary conditions derived in this article are essentially the same as those derived in [3,9], although we propose a slight generalization. The generalization consists of the addition of a parameter in the boundary condition, which allows for more flexibility in the stability proofs of the numerical scheme. In addition, we have not used the simplification of periodicity in the directions tangential to the boundary. We also propose a novel set of pressure based boundary conditions. These sets of boundary conditions are general results and not tied to a specific numerical scheme. (See also [2,4–6,3] for other well-posed boundary conditions and proof of the correct number of boundary conditions to impose.)

Once well-posedness is established, the stability of the discretization is considered, which is the main focus of this article. We rely on the well-known equivalence theorem [7] for linear problems, which roughly speaking says that "a consistent and stable approximation converges to the correct solution as the mesh size goes to zero". Also, in [8] it was shown that linear stability implies stability for the non-linear problem if the solution is smooth.

The theory and numerical techniques used in this article are based on the Summation-by-Parts (SBP) and the Simultaneous Approximation Term (SAT) technique for boundary conditions developed in [10–22]. In [15], stability for SBP–SAT schemes was shown for the one-dimensional Navier–Stokes equations and in [16] stability for a scalar equation was proven in general curvilinear coordinates.

The main result in this article is a proof of stability for the full three-dimensional Navier–Stokes equations in curvilinear coordinates and discretized with high-order SBP–SAT finite difference scheme. (In fact, the discretization is even strictly stable according to the definition in [23].)

2. The Navier–Stokes equations

Let a bar denote a dimensional variable and ∞ denote the free-stream values. We non-dimensionalize the velocities $\bar{u}_1, \bar{u}_2, \bar{u}_3$ using the speed of sound $\bar{a}_\infty$; the density $\rho = \bar{\rho}/\bar{\rho}_\infty$; the temperature $T = \overline{T}/\overline{T}_\infty$; the pressure $p = \bar{p}/(\bar{\rho}_\infty \bar{a}_\infty^2)$ and the total energy $e = \bar{e}/(\bar{\rho}_\infty \bar{a}_\infty^2)$. λ, μ are the second and shear viscosity coefficients non-dimensionalized by $\bar{\mu}_\infty$. q denotes the heat flux and γ is the ratio of the specific heats.

One can derive a few other relations in non-dimensional form: $p_\infty = 1/\gamma$, $a_\infty = 1$, $T_\infty = 1$, $\rho_\infty = 1$, $e_\infty = 1/(\gamma(\gamma-1)) + M^2/2$, where Ma denotes the free-stream Mach-number. The equation of state is $\rho T = \gamma p$. Further,

$$Re = \frac{u_\infty \rho_\infty L}{\mu_\infty}, \quad Ma = \frac{u_\infty}{a_\infty} = u_\infty, \quad Pr = \frac{\mu_\infty c_p}{\kappa_\infty}$$

are the Reynolds number, Mach number and Prandtl number, respectively. u_∞ denotes the magnitude of the free-stream velocity.

We present the governing equations in non-dimensional form and use $\epsilon = M/Re$.

$$\begin{aligned} &u_t + F_x + G_y + H_z = 0, \\ &F = F^I - \epsilon F^V, \quad G = G^I - \epsilon G^V, \quad H = H^I - \epsilon H^V. \end{aligned} \tag{1}$$

A superscript I denotes the inviscid portion of the flux and V the viscous part. The solution and fluxes are defined as follows:

$$
\begin{aligned}
u^{\mathrm{T}} &= (\rho, \rho u_1, \rho u_2, \rho u_3, e),\\
(F^I)^{\mathrm{T}} &= (\rho u_1, p + \rho u_1^2, \rho u_1 u_2, \rho u_1 u_3, u_1(p+e)),\\
(G^I)^{\mathrm{T}} &= (\rho u_2, \rho u_1 u_2, p + \rho u_2^2, \rho u_2 u_3, u_2(p+e)),\\
(H^I)^{\mathrm{T}} &= (\rho u_3, \rho u_1 u_3, \rho u_2 u_3, p + \rho u_3^2, u_3(p+e)),\\
(F^V)^{\mathrm{T}} &= \left(0, \tau_{xx}, \tau_{xy}, \tau_{xz}, u_1\tau_{xx} + u_2\tau_{xy} + u_3\tau_{xz} + \frac{1}{Pr(\gamma-1)}q_x\right),\\
(G^V)^{\mathrm{T}} &= \left(0, \tau_{xy}, \tau_{yy}, \tau_{yz}, u_1\tau_{yx} + u_2\tau_{yy} + u_3\tau_{yz} + \frac{1}{Pr(\gamma-1)}q_y\right),\\
(H^V)^{\mathrm{T}} &= \left(0, \tau_{xz}, \tau_{zy}, \tau_{zz}, u_1\tau_{xz} + u_2\tau_{yz} + u_3\tau_{zz} + \frac{1}{Pr(\gamma-1)}q_z\right).
\end{aligned}
$$

The stress tensor is

$$
\begin{aligned}
\tau_{xx} &= 2\mu\frac{\partial u_1}{\partial x} + \lambda\left(\frac{\partial u_1}{\partial x} - \frac{\partial u_2}{\partial y} - \frac{\partial u_3}{\partial z}\right),\\
\tau_{yy} &= 2\mu\frac{\partial u_2}{\partial y} + \lambda\left(-\frac{\partial u_1}{\partial x} + \frac{\partial u_2}{\partial y} - \frac{\partial u_3}{\partial z}\right),\\
\tau_{zz} &= 2\mu\frac{\partial u_3}{\partial z} + \lambda\left(-\frac{\partial u_1}{\partial x} - \frac{\partial u_2}{\partial y} + \frac{\partial u_3}{\partial z}\right),\\
\tau_{yx} &= \tau_{xy} = \mu\left(\frac{\partial u_1}{\partial y} + \frac{\partial u_2}{\partial x}\right), \quad \tau_{zx} = \tau_{xz} = \mu\left(\frac{\partial u_3}{\partial x} + \frac{\partial u_1}{\partial z}\right),\\
\tau_{zy} &= \tau_{yz} = \mu\left(\frac{\partial u_2}{\partial z} + \frac{\partial u_3}{\partial y}\right).
\end{aligned}
$$

We assume that $3\lambda + 2\mu \geqslant 0$ and in computations we use $\lambda = -2\mu/3$. Throughout this paper, u denotes the conservative variables; v the primitive variables; w the symmetrized variables (after linearization) and c the characteristic variables (also after linearization).

2.1. Curvilinear coordinates

We introduce the coordinate transformation $x = x(\xi,\eta,\zeta)$, $y = y(\xi,\eta,\zeta)$ and $z = z(\xi,\eta,\zeta)$ such that $0 \leqslant \xi,\eta,\zeta \leqslant 1$ and define the Jacobian matrix as

$$
\mathbf{J} = \begin{pmatrix} \frac{\partial x}{\partial \xi} & \frac{\partial x}{\partial \eta} & \frac{\partial x}{\partial \zeta} \\ \frac{\partial y}{\partial \xi} & \frac{\partial y}{\partial \eta} & \frac{\partial y}{\partial \zeta} \\ \frac{\partial z}{\partial \xi} & \frac{\partial z}{\partial \eta} & \frac{\partial z}{\partial \zeta} \end{pmatrix}.
$$

Let $\det(\mathbf{J}) = J$; then the Navier–Stokes equations can be recast as

$$
(Ju)_t + \widehat{F}_\xi + \widehat{G}_\eta + \widehat{H}_\zeta = 0, \tag{2}
$$

where $\widehat{F} = \widehat{F}^I - \epsilon\widehat{F}^V$, $\widehat{G} = \widehat{G}^I - \epsilon\widehat{G}^V$ and $\widehat{H} = \widehat{H}^I - \epsilon\widehat{H}^V$. Furthermore,

$$
\begin{aligned}
\widehat{F}^{I,V} &= J\left(\xi_x F^{I,V} + \xi_y G^{I,V} + \xi_z H^{I,V}\right),\\
\widehat{G}^{I,V} &= J\left(\eta_x F^{I,V} + \eta_y G^{I,V} + \eta_z H^{I,V}\right),\\
\widehat{H}^{I,V} &= J\left(\zeta_x F^{I,V} + \zeta_y G^{I,V} + \zeta_z H^{I,V}\right).
\end{aligned} \tag{3}
$$

For a thorough derivation of the transformed Navier–Stokes equations, see [6].

2.2. The linearized Navier–Stokes equations

So far, we have dealt with the non-linear equations in conservative form. We will employ the energy method to analyze well-posedness of these equations. Therefore, we need a set of linear and symmetric

equations. We transform the Navier–Stokes equations (1) to primitive variables $v = (\rho, u_1, u_2, u_3, p)$ and freeze the coefficients. The tilde sign will denote the time-dependent variable. Variables or matrices without the tilde are the frozen equivalents. Next, we use the symmetrizing matrices, derived in [24], to obtain a system of the form,

$$\begin{aligned}\tilde{w}_t &+ (A_{1w}\tilde{w} - \epsilon(B_{11}\tilde{w}_x + B_{12}\tilde{w}_y + B_{13}\tilde{w}_z))_x + (A_{2w}\tilde{w} - \epsilon(B_{22}\tilde{w}_y + B_{23}\tilde{w}_z + B_{12}\tilde{w}_x))_y \\ &+ (A_{3w}\tilde{w} - \epsilon(B_{33}\tilde{w}_z + B_{32}\tilde{w}_y + B_{13}\tilde{w}_x))_z = 0. \end{aligned} \tag{4}$$

Applying the coordinate transformation described above, we arrive at,

$$(Jw)_t + (\widehat{F}_w)_\xi + (\widehat{G}_w)_\eta + (\widehat{H}_w)_\zeta = 0, \tag{5}$$

where $\widehat{F}_w = \widehat{F}^I_w - \epsilon\widehat{F}^V_w$, $\widehat{G}_w = \widehat{G}^I_w - \epsilon\widehat{G}^V_w$, $\widehat{H}_w = \widehat{H}^I_w - \epsilon\widehat{H}^V_w$, and,

$$\begin{aligned}\widehat{F}^I_w &= J(\xi_x A_{1w} + \xi_y A_{2w} + \xi_z A_{3w})u = \widehat{A}_{1w}w, \\ \widehat{G}^I_w &= J(\eta_x A_{1w} + \eta_y A_{2w} + \eta_z A_{3w})u = \widehat{A}_{2w}w, \\ \widehat{H}^I_w &= J(\zeta_x A_{1w} + \zeta_y A_{2w} + \zeta_z A_{3w})u = \widehat{A}_{3w}w. \end{aligned}$$

The exact forms of $\widehat{F}^V_w, \widehat{G}^V_w$ and $\widehat{H}^V_w$ are found in [6].

Remark. We would arrive at the same system if we had linearized and symmetrized the system (2) directly.

3. Well-posedness

Next, we turn to well-posedness of Eq. (4). Let $D_{\bar{\xi}}$ denote the computational domain and $\Lambda_{\bar{\xi}}$ its boundary, and apply the energy method to (5),

$$\begin{aligned} 0 &= \int_{D_{\bar{\xi}}} \tilde{w}^{\mathrm{T}}\tilde{w}_t J \,\mathrm{d}\xi\,\mathrm{d}\eta\,\mathrm{d}\zeta + \int_{D_{\bar{\xi}}} \tilde{w}^{\mathrm{T}}((\widehat{F}^I_w)_\xi + (\widehat{G}^I_w)_\eta + (\widehat{H}^I_w)_\zeta)\,\mathrm{d}\xi\,\mathrm{d}\eta\,\mathrm{d}\zeta - \epsilon\int_{D_{\bar{\xi}}} \tilde{w}^{\mathrm{T}}((\widehat{F}^V_w)_\xi + (\widehat{G}^V_w)_\eta \\ &\quad + (\widehat{H}^V_w)_\zeta)\,\mathrm{d}\xi\,\mathrm{d}\eta\,\mathrm{d}\zeta \\ &= \int_{D_{\bar{\xi}}} \tilde{w}^{\mathrm{T}}\tilde{w}_t J \,\mathrm{d}\xi\,\mathrm{d}\eta\,\mathrm{d}\zeta + I_1 - \epsilon I_2, \end{aligned} \tag{6}$$

where

$$\begin{aligned} I_1 &= \oint_{\Gamma_{\bar{\xi}}} \frac{1}{2}\left(\tilde{w}^{\mathrm{T}}\left(\widehat{A}_{1w}\right)\tilde{w}, \tilde{w}^{\mathrm{T}}\left(\widehat{A}_{2w}\right)\tilde{w}, \tilde{w}^{\mathrm{T}}\left(\widehat{A}_{3w}\right)\tilde{w}\right)\cdot \mathbf{n}_{\bar{\xi}}\,\mathrm{d}s_{\bar{\xi}} \\ I_2 &= \oint_{\Gamma_{\bar{\xi}}} \tilde{w}^{\mathrm{T}}\widehat{\mathbf{F}}^{\mathbf{V}}\,\mathrm{d}s_{\bar{\xi}} - DI. \end{aligned} \tag{7}$$

where $\mathbf{n}_{\bar{\xi}} = (n_\xi, n_\eta, n_\zeta)$ denotes the outward pointing normal and $\mathrm{d}s_{\bar{\xi}}$ a surface element in $\bar{\xi}$-space. Further, $\widehat{\mathbf{F}}^{\mathbf{V}} = \widehat{F}^V_w n_\xi + \widehat{G}^V_w n_\eta + \widehat{H}^V_w n_\zeta$. DI is a quadratic term in the derivatives of w (see [6]) and is positive semi-definite. We introduce the computational space $D_{\bar{\xi}}$ as $0 \leqslant \xi \leqslant 1$, $0 \leqslant \eta \leqslant 1$, $0 \leqslant \zeta \leqslant 1$. Rewriting (6) using (7) yields

$$\begin{aligned} 2\int_{D_{\bar{\xi}}} \tilde{w}^{\mathrm{T}}\tilde{w}_t J \,\mathrm{d}\xi\,\mathrm{d}\eta\,\mathrm{d}\zeta + 2\epsilon DI &= \int_{\xi=0} \tilde{w}^{\mathrm{T}}\left(\widehat{A}_{1w}\tilde{w} - 2\epsilon\widehat{F}^V_w\right)\mathrm{d}\eta\,\mathrm{d}\zeta + \int_{\xi=1} \tilde{w}^{\mathrm{T}}\left(-\widehat{A}_{1w}\tilde{w} + 2\epsilon\widehat{F}^V_w\right)\mathrm{d}\eta\,\mathrm{d}\zeta \\ &\quad + \int_{\eta=0} \tilde{w}^{\mathrm{T}}\left(\widehat{A}_{2w}\tilde{w} - 2\epsilon\widehat{G}^V_w\right)\mathrm{d}\xi\,\mathrm{d}\zeta + \int_{\eta=1} \tilde{w}^{\mathrm{T}}\left(-\widehat{A}_{2w}\tilde{w} + 2\epsilon\widehat{G}^V_w\right)\mathrm{d}\xi\,\mathrm{d}\zeta \\ &\quad + \int_{\zeta=0} \tilde{w}^{\mathrm{T}}\left(\widehat{A}_{3w}\tilde{w} - 2\epsilon\widehat{H}^V_w\right)\mathrm{d}\xi\,\mathrm{d}\eta + \int_{\zeta=1} \tilde{w}^{\mathrm{T}}\left(-\widehat{A}_{3w}\tilde{w} + 2\epsilon\widehat{H}^V_w\right)\mathrm{d}\xi\,\mathrm{d}\eta. \end{aligned} \tag{8}$$

3.1. Boundary conditions

In order to simplify the analysis we will only study the boundary term at $\xi = 0$ and disregard other boundary terms. Then equation (8) reduces to

$$2\int_{D_{\tilde{\xi}}} \tilde{w}^{\mathrm{T}}\tilde{w}_t J\,\mathrm{d}\xi\,\mathrm{d}\eta\,\mathrm{d}\zeta + 2\epsilon DI - \int_{\xi=0} \tilde{w}^{\mathrm{T}}\left(\widehat{A}_{1w}\tilde{w} - 2\epsilon\widehat{F}_w^V\right)\mathrm{d}\eta\,\mathrm{d}\zeta = 0. \tag{9}$$

We rotate $\widehat{A}_1$ to diagonal form using $X^T\widehat{A}_{1w}X = \Lambda_1$ so that,

$$\Lambda_1 = \mathrm{diag}(u_n, u_n, u_n, u_n + a, u_n - a), \tag{10}$$

where $u_n = (\xi_x u_1 + \xi_y u_2 + \xi_z u_3)/\sqrt{\xi_x^2 + \xi_y^2 + \xi_z^2}$ is the normal component (not necessarily outward pointing) of the velocity through the boundary and a is the speed of sound.

Define $X^{\mathrm{T}}\tilde{w} = \tilde{c}$, i.e $\tilde{c} = (\tilde{c}_1, \tilde{c}_2, \tilde{c}_3, \tilde{c}_4, \tilde{c}_5)^{\mathrm{T}}$ are the characteristic variables and let $X\widehat{F}_w^V = \widehat{F}_c^V$. Note that $\widehat{F}_w^V = (0, \widehat{F}_2^V, \widehat{F}_3^V, \widehat{F}_4^V, \widehat{F}_5^V)^{\mathrm{T}}$. However, $\widehat{F}_c^V$ will be non-zero everywhere. Then,

$$2\int_{D_{\tilde{\xi}}} \tilde{w}^{\mathrm{T}}\tilde{w}_t J\,\mathrm{d}\xi\,\mathrm{d}\eta\,\mathrm{d}\zeta + 2\epsilon DI - \int_{\xi=0} \tilde{c}^{\mathrm{T}}(\widehat{\Lambda}_1\tilde{c} - 2\epsilon\widehat{F}_c^V)\,\mathrm{d}\eta\,\mathrm{d}\zeta = 0. \tag{11}$$

The aim is to use boundary conditions such that a bound on w is obtained. The number of boundary conditions we are allowed to use, are given in Table 1 (see [2,5]).

3.2. Characteristic far-field boundary conditions

There are four different cases, supersonic/subsonic inflow/outflow, with different number of positive eigenvalues of Λ_1. For supersonic inflow ($u_n > a$) there are 5 positive eigenvalues; supersonic outflow ($u_n < -a$), 0 positive; subsonic inflow ($0 < u_n < a$), 4 positive; subsonic outflow ($-a < u_n < 0$), 1 positive. For the Navier–Stokes equations we should use five conditions at an inflow and four at an outflow to bound the following term (see for example [2]).

$$-\int_{\xi=0} \tilde{c}^{\mathrm{T}}\left(\widehat{\Lambda}_1\tilde{c} - 2\epsilon F_c^V\right)\mathrm{d}\eta\,\mathrm{d}\zeta. \tag{12}$$

We split $\Lambda_1 = \Lambda_1^+ + \Lambda_1^-$ holding the positive and negative eigenvalues, respectively, and continue to study the following boundary conditions for supersonic inflow, subsonic inflow and supersonic outflow:

$$\alpha\widehat{\Lambda}_1^+\tilde{c} - \epsilon\widehat{F}_c^V = g^c, \quad \text{or equivalently,} \quad \alpha\widehat{A}_{1w}^+ w - \epsilon\widehat{F}_w^V = g, \tag{13}$$

where we define $\widehat{A}_{1w}^+ = X\widehat{\Lambda}_1^+X^T$ and α is a scalar to be determined for well-posedness. Consider the simplified energy where all terms that do not contribute to a growth of the solution are omitted:

$$\|w\|_t^2 \leqslant \int_{\xi=0} \tilde{c}^{\mathrm{T}}(\widehat{\Lambda}_1^+\tilde{c} - 2\epsilon\widehat{F}_c^V)\,\mathrm{d}\eta\,\mathrm{d}\zeta.$$

We use the boundary condition (13),

$$\|w\|_t^2 \leqslant \int_{\xi=0} \tilde{c}^{\mathrm{T}}(\widehat{\Lambda}_1^+\tilde{c} - 2\epsilon\widehat{F}_c^V)\,\mathrm{d}\eta\,\mathrm{d}\zeta - 2\int_{\xi=0} \tilde{c}^{\mathrm{T}}(\alpha\widehat{\Lambda}_1^+\tilde{c} - \epsilon\widehat{F}_c^V - g^c)\,\mathrm{d}\eta\,\mathrm{d}\zeta \tag{14}$$

and assume that $g = 0$. (We multiply the last integral by 2 to precisely cancel the viscous flux.) That leads to,

Table 1
The number of boundary conditions to be specified at different flow cases and space dimensions (D) for the Navier–Stokes equations

	3D	2D	1D
Sub-/supersonic inflow	5	4	3
Sub-/supersonic outflow	4	3	2

$$\|w\|_t^2 \leqslant (1-2\alpha)\int_{\xi=0} \tilde{c}^{\mathrm{T}}\widehat{\Lambda}_1^+\tilde{c}, \tag{15}$$

which means that $\|w\|_t^2$ is bounded if $\alpha \geqslant 1/2$. It remains to show that the proposed conditions are the minimal number that bound the solution. If not, they do not constitute a well-posed set of boundary conditions.

In the supersonic inflow case all five eigenvalues of Λ_1 are positive; (13) leads to five boundary conditions, which is correct. In the case of supersonic outflow $\Lambda_1^+ = 0$ which leads to the boundary conditions $-\epsilon F^V = g$ where the first component is 0. Hence, we have four boundary conditions, which is the correct number. For subsonic inflow/outflow it is not immediately obvious since they are the sum of two rank deficient conditions. However, it is shown in Appendix A that for a subsonic inflow, (13) constitutes five boundary conditions, which is correct. On the other hand, if we use (13) at a subsonic outflow boundary, we would enforce five linearly independent boundary conditions, which is one too many. In that case, we drop one condition and show that the remaining four bound the solution. We also introduce the auxiliary matrices $\widehat{A}'$ and $\widehat{\Lambda}'$ that impose an extra linearly dependent condition on the remaining equation. (A necessary requirement to later prove stability for the SBP–SAT discretization.) Note also that data must obey the same linear dependence, which is discussed in Appendix A. We summarize these results in the following proposition.

Proposition 3.1. *Let* $X_i^{\mathrm{T}}\widehat{A}_{iw}X_i = \Lambda_i$ *where* $\Lambda_i = \mathrm{diag}(u_n, u_n, u_n, u_n + a, u_n - a)$, $i = 1,2,3$ *and* $u_n = (\chi_x u_1 + \chi_y u_2 + \chi_z u_3)/\sqrt{\chi_x^2 + \chi_y^2 + \chi_3^2}$ *for* $\chi = \xi, \eta, \zeta$, *respectively. Define* $(\widehat{\Lambda}_0')_{5,4} = -(u_n + a)$ *and the remaining components are set to* 0 *and similarly,* $(\widehat{\Lambda}_1')_{4,5} = -(u_n - a)$. *Then at each boundary we have the following sets of linearly well-posed boundary conditions to Eq. (2):*

$$\begin{aligned}
&\text{At } \xi = 0,\ \alpha(\widehat{\Lambda}_1^+ + \widehat{\Lambda}_0')\tilde{c} - \epsilon\widehat{F}_c^V = g_1^c, \qquad \xi = 1,\ \alpha(\widehat{\Lambda}_1^- + \widehat{\Lambda}_1')\tilde{c} - \epsilon\widehat{F}_c^V = g_2^c.\\
&\text{At } \eta = 0,\ \alpha(\widehat{\Lambda}_2^+ + \widehat{\Lambda}_0')\tilde{c} - \epsilon\widehat{G}_c^V = g_3^c, \qquad \eta = 1,\ \alpha(\widehat{\Lambda}_2^- + \widehat{\Lambda}_1')\tilde{c} - \epsilon\widehat{G}_c^V = g_4^c.\\
&\text{At } \zeta = 0,\ \alpha(\widehat{\Lambda}_3^+ + \widehat{\Lambda}_0')\tilde{c} - \epsilon\widehat{H}_c^V = g_5^c, \qquad \zeta = 1,\ \alpha(\widehat{\Lambda}_3^- + \widehat{\Lambda}_1')\tilde{c} - \epsilon\widehat{H}_c^V = g_6^c,
\end{aligned} \tag{16}$$

and $\alpha \geqslant 1/2$.

Remark. For inflow and supersonic outflow it is obvious that the proposed boundary conditions reduce to the characteristic Euler conditions as $\epsilon \to 0$. In Appendix A, it can easily be seen that it holds also at a subsonic outflow.

Remark. Above, we have shown well-posedness, i.e. boundedness of the solution with homogeneous boundary data. However, it is possible to show boundedness of the solution with time-dependent non-zero boundary data. That is usually referred to as *strong well-posedness* (see [23]).

3.3. Pressure boundary condition

The above boundary conditions are the characteristic boundary conditions. In practice, it is sometimes desirable to specify the pressure at the outflow. This can be done in the same framework as the characteristic boundary conditions. We propose to use the form (16) with a specific $\widehat{\Lambda}', \widehat{A}'$.

Proposition 3.2. *Assume that the definitions in Proposition 3.1 hold, and introduce,*

$$\Lambda_0' = \begin{pmatrix} 0 & 0 & 0 & 0 & 0\\ 0 & 0 & 0 & 0 & 0\\ 0 & 0 & 0 & 0 & 0\\ 0 & 0 & 0 & 0 & \lambda_4\\ 0 & 0 & 0 & -\lambda_4 & -\lambda_4 \end{pmatrix}, \quad \Lambda_1' = \begin{pmatrix} 0 & 0 & 0 & 0 & 0\\ 0 & 0 & 0 & 0 & 0\\ 0 & 0 & 0 & 0 & 0\\ 0 & 0 & 0 & -\lambda_5 & -\lambda_5\\ 0 & 0 & 0 & \lambda_5 & 0 \end{pmatrix}, \tag{17}$$

where $\lambda_4 = (u_n + a)$ *and* $\lambda_5 = u_n - a$. *Then (16) is a linearly well-posed set of boundary conditions to Eq. (2), that specify pressure and viscous gradients.*

Proof. See Appendix B. □

4. Discretization

The above analysis of well-posedness is based on an energy estimate of the solution. To discretize the equations we use high-order finite difference schemes that satisfies a Summation-by-Parts property (SBP) together with the Simultaneous Approximation Term technique to impose boundary conditions. This allows us to prove stability with discrete energy estimates that mimics the continuous analysis.

4.1. Difference operators

Discretize $0 \leqslant x \leqslant 1$ using $N+1$ evenly distributed grid points with spacing h. Introduce the scalar grid function $v(t) = (v_0(t), \ldots, v_N(t))^{\mathrm{T}}$. Then the first derivative is approximated by, $P^{-1}Qv$, where P is a positive definite (symmetric) matrix. P is used to define a discrete l_2 equivalent norm, $\|v\|_P^2 = v^{\mathrm{T}}Pv$. In our particular schemes P is diagonal which is a necessary requirement for stability on curvilinear grids. (See [19].) Q is skew-symmetric except at the corners and $Q + Q^{\mathrm{T}} = \mathrm{diag}(-1, 0, \ldots, 0, 1) = B$.

We will use Kronecker products (denoted $\otimes$) to formulate our scheme (see for example [25] for a definition). Let solution field be u^{ijkl} where the indices represent variable, ξ, η and ζ index. The last index ranges between 1 and 5. The spatial indices between, $0, \ldots, n_\xi$, $0, \ldots, n_\eta$ and $0, \ldots, n_\zeta$. Order a vector $\mathbf{u} = (u^{0001}, u^{0002}, \ldots, u^{n_\xi, n_\eta, n_\zeta, 5})^{\mathrm{T}}$. The finite difference matrices are

$$\mathbf{D}_{\boldsymbol{\xi}} = (I_\zeta \otimes I_\eta \otimes D_\xi \otimes I_5), \quad \mathbf{D}_{\boldsymbol{\eta}} = (I_\zeta \otimes D_\eta \otimes I_\xi \otimes I_5), \quad \mathbf{D}_{\boldsymbol{\zeta}} = (D_\zeta \otimes I_\eta \otimes I_\xi \otimes I_5).$$

All submatrices appearing in the first position are of size $(n_\zeta + 1) \times (n_\zeta + 1)$, the second position $(n_\eta + 1) \times (n_\eta + 1)$, the third position $(n_\xi + 1) \times (n_\xi + 1)$ and the fourth position 5×5. I with subscript denotes an identity matrix. We will also need,

$$\mathbf{B}_{\boldsymbol{\xi}} = (I_\zeta \otimes I_\eta \otimes B_\xi \otimes I_5), \quad \mathbf{B}_{\boldsymbol{\eta}} = (I_\zeta \otimes B_\eta \otimes I_\xi \otimes I_5), \quad \mathbf{B}_{\boldsymbol{\zeta}} = (B_\zeta \otimes I_\eta \otimes I_\xi \otimes I_5),$$

where $B_{\xi,\eta,\zeta} = \mathrm{diag}(-1, 0, \ldots, 0, 1)$ with appropriate sizes. (c.f Section 4.1 for the definition.) In the same way,

$$\mathbf{Q}_{\boldsymbol{\xi}} = (I_\zeta \otimes I_\eta \otimes Q_\xi \otimes I_5), \quad \mathbf{Q}_{\boldsymbol{\eta}} = (I_\zeta \otimes Q_\eta \otimes I_\xi \otimes I_5), \quad \mathbf{Q}_{\boldsymbol{\zeta}} = (Q_\zeta \otimes I_\eta \otimes I_\xi \otimes I_5),$$
$$\mathbf{P}_{\boldsymbol{\xi}} = (I_\zeta \otimes I_\eta \otimes P_\xi \otimes I_5), \quad \mathbf{P}_{\boldsymbol{\eta}} = (I_\zeta \otimes P_\eta \otimes I_\xi \otimes I_5), \quad \mathbf{P}_{\boldsymbol{\zeta}} = (P_\zeta \otimes I_\eta \otimes I_\xi \otimes I_5),$$
$$\mathbf{P}_{\boldsymbol{\xi\eta}} = \mathbf{P}_{\boldsymbol{\xi}}\mathbf{P}_{\boldsymbol{\eta}}, \quad \mathbf{P}_{\boldsymbol{\eta\zeta}} = \mathbf{P}_{\boldsymbol{\eta}}\mathbf{P}_{\boldsymbol{\zeta}}, \quad \mathbf{P}_{\boldsymbol{\xi\zeta}} = \mathbf{P}_{\boldsymbol{\xi}}\mathbf{P}_{\boldsymbol{\zeta}}\mathbf{P} = \mathbf{P}_{\boldsymbol{\xi}}\mathbf{P}_{\boldsymbol{\eta}}\mathbf{P}_{\boldsymbol{\zeta}}.$$

We define $E_0 = \mathrm{diag}(1, 0, 0, \ldots)$ and $E_1 = \mathrm{diag}(\ldots, 0, 0, 1)$ with sizes consistent with their appearances in the Kronecker products. Moreover, $\mathbf{E}_{\mathbf{0}\boldsymbol{\xi}} = (I_\zeta \otimes I_\eta \otimes E_0)$ and $\mathbf{E}_{\mathbf{1}\boldsymbol{\xi}}, \mathbf{E}_{\mathbf{0},\boldsymbol{\eta}}, \ldots$ are defined similarly. Finally, we introduce the norm $\mathbf{u}^{\mathrm{T}}\mathbf{P}\mathbf{u} = \|\mathbf{u}\|^2$.

Remark. Note that the Kronecker products used is merely a theoretical tool. When implementing the scheme one may view the different operators in a Kronecker product as operating in their own dimension, i.e on a specific index. To compute $\mathbf{D}_\eta\mathbf{u}$, we view $\mathbf{u}$ as a field with four indices and the one-dimensional operator D_η will operate on the second index since it appears at the second position in the Kronecker product for all combinations of the other indices. That is exactly as one would normally code a finite difference scheme, i.e. loop over ξ, ζ and variables.

4.2. Stability of the Navier–Stokes equations

We begin by deriving an energy estimate. All other boundaries are assumed to be stable with correct boundary conditions (and will be omitted) except the one at $\xi = 0$. We do not introduce the boundary conditions at $\xi = 0$ initially. They will be derived through the stability analysis and introduced as penalty terms.

Denote by $\mathbf{u}(t)$ the solution vector with components $u^{ijkl}(t)$ (ordered as described previously) approximating the exact solution $u_l(\xi_i, \eta_j, \zeta_k, t)$ where u_l is the component of the variables in conservative form. In the same

manner we define the inviscid flux vectors, $\mathbf{F^I}, \mathbf{G^I}, \mathbf{H^I}$ and the viscous flux vectors $\mathbf{F^V}, \mathbf{G^V}, \mathbf{H^V}$ with components $F^{I,ijkl}$, etc. Finally, $\mathbf{Ju}$ has components $J(\xi_i, \eta_j, \zeta_k)u^{ijkl}$. Note that J is positive for all i,j,k. Then,

$$(\mathbf{Ju})_t + \mathbf{D}_\xi(\mathbf{F^I} - \epsilon\mathbf{F^V}) + \mathbf{D}_\eta(\mathbf{G^I} - \epsilon\mathbf{G^V}) + \mathbf{D}_\zeta(\mathbf{H^I} - \epsilon\mathbf{H^V}) = \mathbf{0}. \tag{18}$$

As in the continuous case we transform to primitive variables and freeze the coefficients. Apply the symmetrizing matrices to obtain,

$$(\mathbf{Jw})_t + \mathbf{D}_\xi(\mathbf{F^I_w} - \epsilon\mathbf{F^V_w}) + \mathbf{D}_\eta(\mathbf{G^I_w} - \epsilon\mathbf{G^V_w}) + \mathbf{D}_\zeta(\mathbf{H^I_w} - \epsilon\mathbf{H^V_w}) = \mathbf{0}, \tag{19}$$

where the exact form of the viscous fluxes in curvilinear coordinates can be found in [6]. The derivatives in the viscous fluxes are computed with $\mathbf{D}_\xi$, $\mathbf{D}_\eta$ and $\mathbf{D}_\zeta$. We now apply the energy method to (18).

$$\mathbf{w}^{\mathrm{T}}\mathbf{P}(\mathbf{Jw})_t + \mathbf{w}^{\mathrm{T}}\mathbf{Q}_\xi\mathbf{P}_{\eta\zeta}(\mathbf{F^I_w} - \epsilon\mathbf{F^V_w}) + \mathbf{w}^{\mathrm{T}}\mathbf{Q}_\eta\mathbf{P}_{\xi\zeta}(\mathbf{G^I_w} - \epsilon\mathbf{G^V_w}) + \mathbf{v}^{\mathrm{T}}\mathbf{Q}_\zeta\mathbf{P}_{\xi\eta}(\mathbf{H^I_w} - \epsilon\mathbf{H^V_w}) = 0$$

or,

$$\|\sqrt{\mathbf{J}}\mathbf{w}\|^2_{\mathbf{t}} + \mathbf{w}^{\mathrm{T}}\mathbf{B}_\xi\mathbf{P}_{\eta\zeta}(\widehat{\mathbf{A}}_{\mathbf{1w}}\mathbf{w} - \mathbf{2}\epsilon\mathbf{F^V_w}) + \mathbf{w}^{\mathrm{T}}\mathbf{B}_\eta\mathbf{P}_{\xi\zeta}(\widehat{\mathbf{A}}_{\mathbf{2w}}\mathbf{w} - \mathbf{2}\epsilon\mathbf{G^V_w}) + \mathbf{w}^{\mathrm{T}}\mathbf{B}_\zeta\mathbf{P}_{\xi\eta}(\widehat{\mathbf{A}}_{\mathbf{3w}}\mathbf{w} - \mathbf{2}\epsilon\mathbf{H^V_w}) + \mathbf{2}\epsilon\mathbf{DI} = 0. \tag{20}$$

We define $\widehat{\mathbf{A}}_{\mathbf{iw}} = (I_\zeta \otimes I_\eta \otimes I_\zeta \otimes A_{iw})$. $\mathbf{DI}$ denotes a quadratic term in the first-derivative difference approximations of the solution as in (8), and can be proven positive semi-definite. In fact, Eq. (20) corresponds exactly to (8). $\mathbf{B}_{\xi,\eta,\zeta}$ picks out the boundary terms in each direction. Only one of the 6 boundary terms will be non-zero at each boundary. To keep the algebra to a minimum we focus on $\xi = 0$ and disregard the boundary terms:

$$\|\sqrt{\mathbf{J}}\mathbf{w}\|^2_{\mathbf{t}} - \mathbf{w}^{\mathrm{T}}\mathbf{P}_{\eta\zeta}(\widehat{\mathbf{A}}_{\mathbf{1w}}\mathbf{w} - \mathbf{2}\epsilon\mathbf{F^V_w})|_{\xi=\mathbf{0}} + \mathbf{2}\epsilon\mathbf{DI} = 0.$$

We transform the boundary term to characteristic form with $\sum_{m=1}^{5} X_{lm} w^{ijkm} = c^{ijkl}$ and $\sum_{m=1}^{5} X_{lm}\widehat{F}^{V,ijkm}_w = \tilde{G}^{V,ijkl}_c$,

$$\|\sqrt{\mathbf{J}}\mathbf{w}\|^2_{\mathbf{t}} + \mathbf{c}^{\mathrm{T}}\mathbf{P}_{\eta\zeta}(\widehat{\mathbf{\Lambda}}_{\mathbf{1}}\mathbf{c} - \mathbf{2}\epsilon\tilde{\mathbf{G}}^{\mathbf{V}}_{\mathbf{c}})|_{\xi=\mathbf{0}} + \mathbf{2}\epsilon\mathbf{DI} = 0,$$

or, stated as a Kronecker product,

$$\|\sqrt{\mathbf{J}}\mathbf{w}\|^2_{\mathbf{t}} - \mathbf{c}^{\mathrm{T}}(E_0 \otimes P_\eta \otimes P_\zeta \otimes \Lambda_1)\mathbf{c} + 2\epsilon\mathbf{c}^{\mathrm{T}}(E_0 \otimes P_\eta \otimes P_\zeta \otimes I_5)\tilde{\mathbf{G}}^{\mathbf{V}}_{\mathbf{c}} + \mathbf{DI} = 0. \tag{21}$$

We define $\mathbf{\Lambda}^+_{\mathbf{1}} = (I_\xi \otimes I_\eta \otimes I_\zeta \otimes \Lambda^+_1)$. For inflow and supersonic outflow we construct a term,

$$\text{penalty} = 2\sigma^I\mathbf{c}^{\mathrm{T}}\mathbf{E}_{\mathbf{0}\xi}\left(\mathbf{P}_{\eta\zeta}\mathbf{\Lambda}^+_{\mathbf{1}}\left(\mathbf{c} - \mathbf{g^I_c}\right)\right) + 2\epsilon\sigma^V\mathbf{c}^{\mathrm{T}}\mathbf{E}_{\mathbf{0}\xi}\mathbf{P}_{\eta\zeta}(\mathbf{G^V} - \mathbf{g^V_c}). \tag{22}$$

that is zero to within truncation error. If (22) is added to (21) the energy may be bounded for certain choices of σ^I and σ^V. To prove stability it is sufficient to consider the case $g^I_c = g^V_c = 0$. We obtain,

$$\begin{aligned}\|\sqrt{\mathbf{J}}\mathbf{w}\|^2_{\mathbf{t}} &- (1 + 2\sigma^I)\mathbf{c}^{\mathrm{T}}(E_{0\xi} \otimes P_\eta \otimes P_\zeta \otimes \Lambda^+_1)\mathbf{c} - \mathbf{c}^{\mathrm{T}}(E_{0\xi} \otimes P_\eta \otimes P_\zeta \otimes \Lambda^-_1)\mathbf{c} \\ &+ 2(1 - \sigma^V)\epsilon\mathbf{c}^{\mathrm{T}}(E_{0\xi} \otimes P_\eta \otimes P_\zeta \otimes I_5)\tilde{\mathbf{G}}^{\mathbf{V}}_{\mathbf{c}} + \mathbf{2}\epsilon\mathbf{DI} = 0.\end{aligned} \tag{23}$$

It is clear from (23) that $\sigma^I \leqslant -1/2$ and $\sigma^V = 1$ bounds the energy. Moreover, the penalty term in (22) can be written as

$$\text{penalty} = -2\sigma^V\mathbf{E}_{\mathbf{0}\xi}\mathbf{P}_{\eta\zeta}(\alpha\mathbf{\Lambda}^+_{\mathbf{1}}\mathbf{c} - \epsilon\mathbf{G^V_c} - \mathbf{g_c}), \tag{24}$$

where $\alpha = -\frac{\sigma^I}{\sigma^V}$ and $\mathbf{g_c} = (\mathbf{\Lambda}^+_{\mathbf{1}}\mathbf{g^I_c} + \mathbf{g^V_c})$. Eq. (24) shows that the penalty terms are exactly the boundary condition proposed for super- and subsonic inflow and supersonic outflow. The conditions for stability require $\alpha \geqslant 1/2$ which is in accordance with the theory for well-posedness.

For subsonic outflow we replace $\mathbf{\Lambda}^+_{\mathbf{1}}$ with $\Lambda^+_1 + \mathbf{\Lambda}'$ and stability follows from the same analysis resulting in the same conditions on the penalty parameters σ^I and σ^V. This can be realized in the following way. If the equation is split into its five components and the analysis carried out for the first four, i.e. for a reduced

Λ^+, Λ' will only introduce a change in the 5th equation making it linearly dependent of the first four. If those are bounded, the 5th equation can shown to be bounded in a similar way as in the continuous case.

Having derived penalty terms to be added to the energy and shown that the proposed penalties enforces the correct boundary conditions, we return to the original system. We obtain,

$$\begin{aligned}&(\mathbf{Jw})_t + \mathbf{D}_\xi(\mathbf{F}^{\mathbf{I}}_{\mathbf{w}} - \epsilon\mathbf{F}^{\mathbf{V}}_{\mathbf{w}}) + \mathbf{D}_\eta(\mathbf{G}^{\mathbf{I}}_{\mathbf{w}} - \epsilon\mathbf{G}^{\mathbf{V}}_{\mathbf{w}}) + \mathbf{D}_\zeta(\mathbf{H}^{\mathbf{I}}_{\mathbf{w}} - \epsilon\mathbf{H}^{\mathbf{V}}_{\mathbf{w}})\\ &\quad = \mathbf{P}^{-1}_\xi\mathbf{E}_{\mathbf{0}\xi}(\sigma^I\widehat{\mathbf{A}}^{\mathbf{in}}_{\mathbf{1w}}(\mathbf{w} - \mathbf{g}^{\mathbf{I}}_{\mathbf{w}}) + \sigma^V\epsilon(\mathbf{F}^{\mathbf{V}}_{\mathbf{w}} - \mathbf{g}^{\mathbf{V}}_{\mathbf{w}})),\end{aligned} \tag{25}$$

where $\widehat{\mathbf{A}}^{\mathbf{in},+}_{\mathbf{1w}}$ denotes $\widehat{A}^+_{1w}$ on inflows and supersonic outflows, or $\widehat{\mathbf{A}}^+_{\mathbf{1w}} + \widehat{\mathbf{A}}'_{\mathbf{1w}}$ on subsonic outflows. (***in*** signifying that it is the inflow part of $\widehat{\mathbf{A}}_{\mathbf{1w}}$.) Similarly, we define $\widehat{\mathbf{A}}^{\mathbf{in},-}_{\mathbf{1w}}$ as $\widehat{A}^-_{1w}$ or $\widehat{\mathbf{A}}^-_{\mathbf{1w}} + \widehat{\mathbf{A}}'_{\mathbf{1w}}$ on subsonic outflow. Finally, we state the entire non-linear scheme with penalty terms for all boundaries:

$$\begin{aligned}&(\mathbf{Ju})_t + \mathbf{D}_\xi(\mathbf{F}^{\mathbf{I}} - \epsilon\mathbf{F}^{\mathbf{V}}) + \mathbf{D}_\eta(\mathbf{G}^{\mathbf{I}} - \epsilon\mathbf{G}^{\mathbf{V}}) + \mathbf{D}_\zeta(\mathbf{H}^{\mathbf{I}} - \epsilon\mathbf{H}^{\mathbf{V}})\\ &\quad = \mathbf{P}^{-1}_\xi\mathbf{E}_{\mathbf{0}\xi}(\sigma^I_0\widehat{\mathbf{A}}^{\mathbf{in},+}_{\mathbf{1}}(\mathbf{w} - \mathbf{g}^{\mathbf{I}}) + \sigma^V_0\epsilon(\mathbf{F}^{\mathbf{V}} - \mathbf{g}^{\mathbf{V}})) + \mathbf{P}^{-1}_\xi\mathbf{E}_{\mathbf{1}\xi}(\sigma^I_1\widehat{\mathbf{A}}^{\mathbf{in},-}_{\mathbf{1}}(\mathbf{w} - \mathbf{g}^{\mathbf{I}}) + \sigma^V_1\epsilon(\mathbf{F}^{\mathbf{V}} - \mathbf{g}^{\mathbf{V}}))\\ &\qquad + \mathbf{P}^{-1}_\eta\mathbf{E}_{\mathbf{0}\eta}(\sigma^I_0\widehat{\mathbf{A}}^{\mathbf{in},+}_{\mathbf{2}}(\mathbf{w} - \mathbf{g}^{\mathbf{I}}) + \sigma^V_0\epsilon(\mathbf{G}^{\mathbf{V}} - \mathbf{g}^{\mathbf{V}})) + \mathbf{P}^{-1}_\eta\mathbf{E}_{\mathbf{1}\eta}(\sigma^I_1\widehat{\mathbf{A}}^{\mathbf{in},-}_{\mathbf{2}}(\mathbf{w} - \mathbf{g}^{\mathbf{I}}) + \sigma^V_1\epsilon(\mathbf{G}^{\mathbf{V}} - \mathbf{g}^{\mathbf{V}}))\\ &\qquad + \mathbf{P}^{-1}_\zeta\mathbf{E}_{\mathbf{0}\zeta}(\sigma^I_0\widehat{\mathbf{A}}^{\mathbf{in},+}_{\mathbf{3}}(\mathbf{w} - \mathbf{g}^{\mathbf{I}}) + \sigma^V_0\epsilon(\mathbf{H}^{\mathbf{V}} - \mathbf{g}^{\mathbf{V}})) + \mathbf{P}^{-1}_\zeta\mathbf{E}_{\mathbf{1}\zeta}(\sigma^I_1\widehat{\mathbf{A}}^{\mathbf{in},-}_{\mathbf{3}}(\mathbf{w} - \mathbf{g}^{\mathbf{I}}) + \sigma^V_1\epsilon(\mathbf{H}^{\mathbf{V}} - \mathbf{g}^{\mathbf{V}})).\end{aligned} \tag{26}$$

The penalty parameters that lead to a stable scheme are listed in Table 2. The marginal values $\sigma^I_0 = -1/2$ and $\sigma^I_1 = 1/2$ correspond to the minimally dissipative case and $\sigma^I_0 = -1$ and $\sigma^I_1 = 1$ are equivalent to specifying the total fluxes.

Remark. Note also that there is an ambiguity in the definition of the matrices $\widehat{A}_{1,2,3}$. In the linear theory we assumed that they were constant but in the non-linear computation they are not. Hence, they may either be constructed from data, from the solution or a combination of both. We stress that any of these are valid in the linear sense and lead to a stable scheme. Our computational experience indicates, that for smooth solutions the choice is less important and the scheme is stable for the all the different choices. However, we choose them to be the Roe-averages, i.e. $\widehat{F}^I(u) - \widehat{F}^I(g^i) = \widehat{A}_1(u, g^I)(u - g^I)$, which may be advantageous in an extension to allow for non-smooth solutions.

Remark. An important property of the non-linearity is that the boundary conditions are applied locally. It is not necessary to a-priori specify if it is a sub- or supersonic inflow or outflow. The choice of eigenvalues is a local operation at each gridpoint on the boundary and in the case of subsonic outflow, the auxiliary matrix is added.

Remark. The symmetric form of the linearized equations serves as an analytical tool to derive well-posed boundary conditions. In a program it is more convenient to transform the boundary terms to the characteristic form directly from the conservative formulation. See for example [26].

Remark. In [9], a set of boundary conditions with the special choice $\alpha = 1$ were derived. They use the penalty technique in the context of spectral methods. However, with $\alpha = 1$ they have less flexibility in the choice of penalty parameters.

5. Computations

The code was shown to have global order of accuracy 3, 4 and 5 in [22].

Table 2
Stable choices of penalty parameters

$\xi, \eta, \zeta = 0$		$\xi, \eta, \zeta = 1$	
$\sigma^I_0 \leqslant -\frac{1}{2}$	$\sigma^V_0 = 1$	$\sigma^I_1 \geqslant \frac{1}{2}$	$\sigma^V_1 = -1$

5.1. Vortex hitting outflow boundary

In realistic computations it is common that flow structures are swept downstream and approach an outflow boundary that ideally should be totally transparent in order to model the free space. So far, we have addressed the question of choosing boundary conditions and we have proposed a well-posed set. This means that whatever data we choose to supply, there is a unique solution. If we want the outflow to mimic free space we have no choice but to supply it with the exact free space solution. However, that solution is rarely known. We have to guess the data to the best of our knowledge and hence our solution will deviate from the true free space solution. The mismatch will appear as waves reflecting from the outflow boundary. With given "erroneous" data, the boundary conditions may be more or less reflective. The present choice can be shown to be a low-order Engquist–Majda condition, see [27].

To test the stability of the outflow boundary conditions, we will study a case where an isentropic vortex hits the outflow boundary. The vortex is an analytical solution to the inviscid Euler equations:

$$\begin{aligned} &\rho = 1 - (x - x_0) - (Mt)^2 - (y - y_0)^2, \quad u = M - \frac{\delta(y - y_0)}{2\pi}\exp(f/2), \\ &v = \frac{\delta(x - x_0 - Mt)}{2\pi}\exp(f/2), \quad f = 1 - ((x - x_0) - Mt)^2 - (y - y_0)^2, \\ &p = \frac{\rho^\gamma}{\gamma}. \end{aligned} \tag{27}$$

The parameter δ is the vortex strength and Ma is the Mach number. Unless otherwise stated we use $\delta = 0.5$. In the case of the Navier–Stokes equations it will dissipate and deviate from the inviscid solution.

We will compute two different cases. The first will use the Euler solution as boundary data. This is not the exact solution for the Navier–Stokes equations and the difference increase with decreasing Reynolds number and longer time. The other test case uses homogeneous free-stream boundary data on the outflow. This is of course very far from the free-space solution when the vortex hits the boundary.

We use a Cartesian grid on $x = 0, \ldots, 10, y = 0, \ldots, 20$, with 101×201 grid points. Reynolds number is 500 and the Mach number is 0.5. The vortex is placed at $x = 5, y = 10$ at $t = 0$, see Fig. 1. We run the computations until $t = 20$. In an inviscid calculation, the center of the vortex would be at $x = 15$, well outside the computational domain. Inside the computational domain the solution would be very close to free-stream. In the Navier–Stokes case it will be very similar although the vortex should have dissipated somewhat. Hence, we compute the maximum deviation from free-stream as a measure of the sizes of the reflections on the outflow boundary. In neither of the computations is artificial dissipation used (see Fig. 2).

In Table 3, we list the free-stream values and the maximum deviation from free-stream in the initial conditions. We use the deviations in each variable at $t = 0$ to normalize the deviations from free stream at $t = 20$, as a measure of the relative errors of the reflections. To show what numerical errors the numerical scheme itself produces we compute the vortex solution using the Euler equations, the exact solution as boundary data and a third-order accurate scheme. The errors at $t = 20$ when the vortex has passed through the boundary is displayed in Table 4. As is seen the numerical errors even for a third-order scheme are very small on this grid. The characteristic boundary conditions are virtually transparent and the vortex passes through the boundary with very small reflections when exact data are used. For completeness, we also include convergence studies in Table 5 for the third- and the fifth-order schemes at $t = 20$ (the two schemes used below).

Next, we turn to the first test case for the Navier–Stokes equations. We compute the solution from $t = 0 - 20$ with the third-order scheme using the Euler solution as boundary data. Note that we do not have the exact data. The errors due to reflections at the boundary are shown in Table 6. Although the boundary data differ from the exact free-stream solution, the reflections are small.

The final and most severe test for the boundary conditions is the one with free-stream values as boundary data. The numerical solution is remarkably stable just as the theory predicts and the reflective errors are displayed in Table 7. The absolute level of the errors are of the same order for all variables and smaller than the initial disturbances. The initial deviation in ρ is an order of magnitude smaller than the other variables implying a large relative error in ρ at $t = 20$.

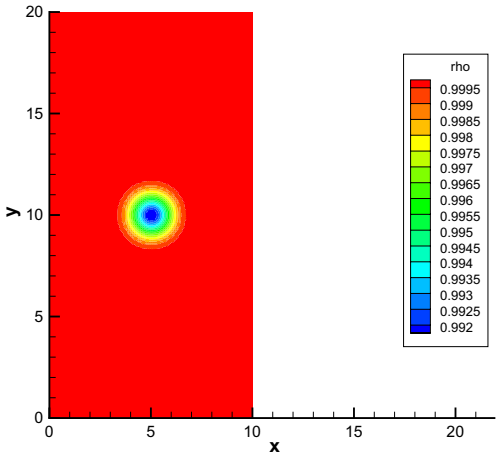

Fig. 1. The initial condition for ρ.

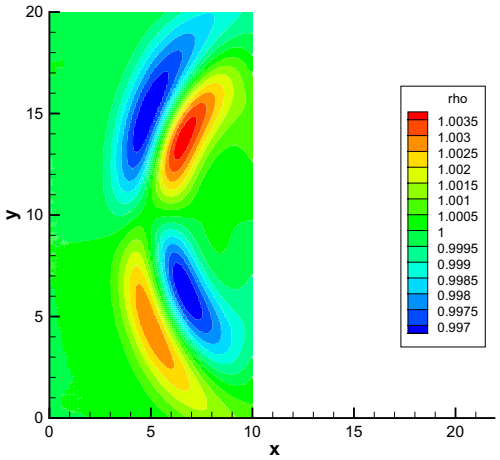

Fig. 2. ρ at $t = 20$ with free-stream boundary data. Note that scale is different from Fig. 1.

Table 3
Free-stream values of variables and initial perturbation from free-stream

Variable	Free-stream	Perturbation $t = 0$
ρ	1	0.009
ρu	0.5	0.08
ρv	0	0.08
e	1.91	0.05

Table 4
Maximum errors and relative errors for the Euler vortex at $t = 20$ computed with Euler equations and exact boundary data

Variable	Absolute error	Relative error (%)
ρ	$1.5e-5$	0.17
ρu	$3.2e-5$	0.04
ρv	$9.2e-5$	0.12
e	$5.1e-5$	0.10

Table 5
Convergence study for the Euler vortex at $t = 20$ computed with Euler equations and exact boundary data

Grid	e_3	q_3	e_5	q_5
26×51	4.0e − 4	–	6.2e-4	–
51×101	4.7e − 5	3.1	1.8e − 5	5.2
101×201	5.6e − 6	3.1	4.1e − 7	5.4

Table 6
Perturbation from free-stream at $t = 20$, computed using the Navier–Stokes equations

Variable	Absolute error	Relative error (%)
ρ	1.3e − 4	1.4
ρu	1.1e − 4	0.13
ρv	2.1e − 4	0.26
e	2.7e − 4	0.54

Absolute value and percent of initial perturbation. Euler vortex boundary data.

Table 7
Perturbation from free-stream at $t = 20$, computed with the Navier–Stokes equations

Variable	Absolute error	Relative error (%)
ρ	3.7e − 3	41
ρu	1.8e − 3	2.3
ρv	2.1e − 3	2.6
e	8.4e − 3	17

Absolute value and percent of initial perturbation. Free-stream boundary data on outflow.

We also obtained (almost) identical errors with the following numerical set-ups: (1) a (51×101)-grid for the third-order method; (2) the 101×201-grid with the fifth-order scheme; (3) a (51×101)-grid and the fifth-order scheme. This shows that the reflections are due to the mismatch of data and not numerical errors.

To test the sensitivity in the reflections with respect to vortex strength, we ran the third-order scheme with vortex strengths $\delta = 0.25$ and $\delta = 1.0$ and concluded that the relative errors due to the reflections were of the same order. As a test of robustness, we ran vortex strength $\delta = 5.0$, which is so strong that backflow occurs. The reflections are substantial with relative errors of order one, but the computation was perfectly stable and no artificial dissipation was needed.

Finally, we tested the effect of the parameter α in the boundary condition (and $\delta = 0.5$). With $\alpha = 0.5$ and $\alpha = 1.0$ the reflections were almost identical, while with $\alpha = 2$ the errors were notably larger. Again, both computations were stable without addition of artificial dissipation.

Remark. The purpose of the above tests are twofold. Firstly, to show that the boundary treatment is very robust. Secondly, to show the sizes of the reflections one obtains due to the mismatch of data. We stress that the boundary conditions were not derived to be minimally reflective.

5.2. Vortex shedding behind cylinder

We will now compute the 3D solution to a cylinder in free-stream. We use a multiblock grid with $101 \times 131 \times 20$ grid points in each of the five computational blocks, see Fig. 3. The z-axis is aligned with the cylinder. Without going into details, we conclude that the interfaces can be treated in a stable manner and refer to [14–16] and an upcoming article by the present authors. The wall boundary can also be treated with a penalty technique but we postpone that discussion to a subsequent article.

We use Reynolds number 500, Mach number 0.5 and Prandtl number 0.72. Again, we want to demonstrate the robustness of the far-field boundary conditions. We initialize the flow by inserting the Euler vortex (from previous section) in front of the cylinder at $x = -2, y = 0$. The z-direction is periodic. The Euler vortex initiates the vortex shedding. The free-stream is aligned with the x-axis for the initial condition. However,

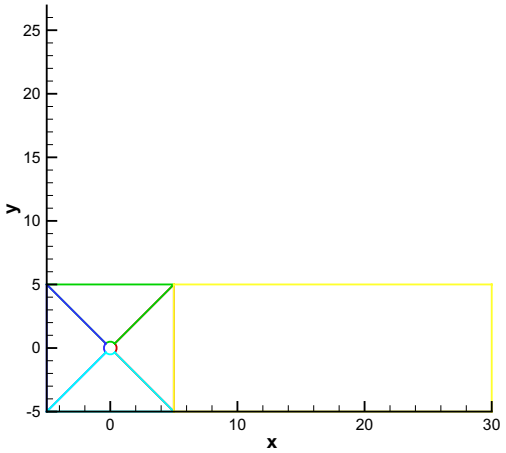

Fig. 3. The five-block computational grid for the cylinder.

when the computation starts, we shift the direction of the free-stream to an angle of 10° in the xz-plane. This change will only affect the interior solution via the boundary conditions. At first, the initial and boundary conditions are incompatible and it is a severe test of the robustness. Indeed, this test poses no problem for the numerical scheme. The solution for the ρw variable (momentum in the z-direction) is shown in Fig. 4 at $t = 20$ in the plane $z = 0$. The upper and lower boundaries are incompatible initially, which produce the waves

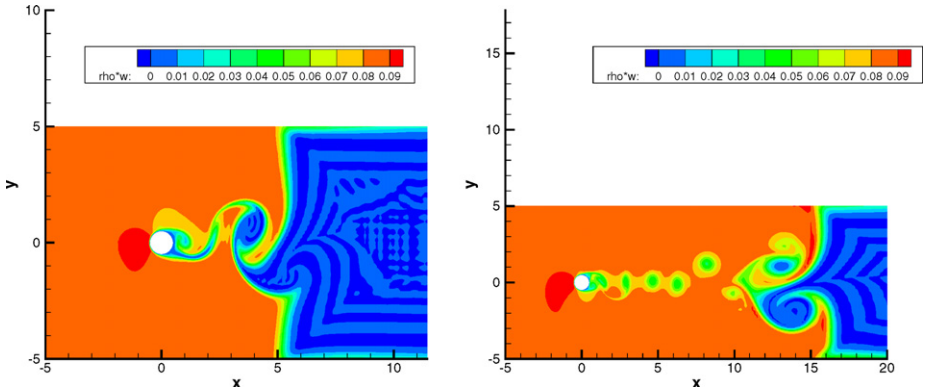

Fig. 4. Left: ρw at $t = 20$. Right: ρw at $t = 40$.

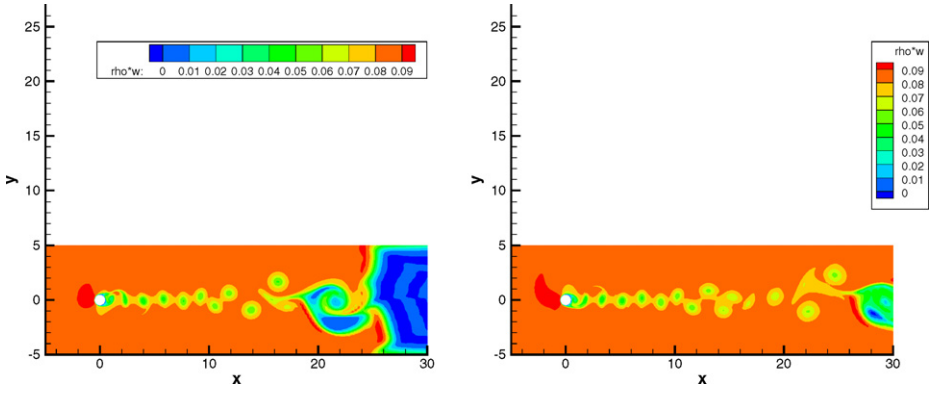

Fig. 5. Left: ρw at $t = 60$. Right: ρw at $t = 80$.

aligned with the x-axis. F
The wave front from the

In Figs. 4–6, the time
travels downstream and

Another feature with
along the same boundar
positive and negative va
gerated since the contou

In this boundary t
accordingly.

This test case is cho
order to accurately con

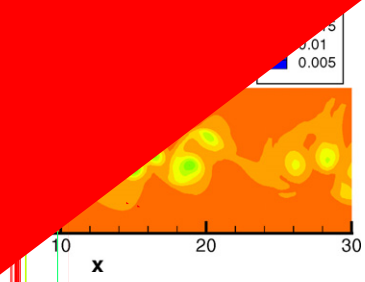

Fig. 6. ρw at $t = 100$.

data. However, if we run this case for sufficiently long time the initial transients will eventually decay and a stable vortex shedding will be observed. In realistic applications, this is a common way to compute the solution and the most critical part, from a stability perspective, is the initial phase with incompatible data. With this example, we have shown that even with a high-order method this is a feasible approach.

6. Conclusions

We have derived a well-posed set of boundary conditions, which is a generalization of the boundary conditions derived in [3,9]. In the subsonic outflow case we derived a different formulation of the boundary conditions that enforces the four conditions on all five equations. For completeness, we also derived a novel set of subsonic outflow conditions using the pressure.

We used these boundary conditions in high-order SBP–SAT finite difference schemes and the main results in this article was a stability proof for the full three-dimensional Navier–Stokes equations in general curvilinear coordinates. These schemes have theoretically second-,third-, fourth and fifth-order accuracy.

The robustness of the boundary conditions was tested in a two-dimensional case where a vortex hit a subsonic outflow boundary. Different boundary data was chosen, which induced reflections of different sizes. In all cases the code was stable.

Finally, we computed the three-dimensional vortex shedding behind a cylinder in an oblique free-stream. We showed that the large structures pass out through the outflow boundary.

The boundary treatment does not require that a boundary is assigned to be either inflow or outflow, sub or supersonic. Instead, the boundary type is determined by the local eigenvalues. This were also highlighted in the computations, where both subsonic inflow and outflow occur on the same boundary.

Acknowledgments

The authors thank Dr. Nail Yamaleev at North Carolina A&T State University and Dr. Ardeshir Hanifi at the Swedish Defence Research Agency for their support of this project.

Appendix A. Subsonic inflow and outflow

Let, a denotes the speed of sound and $\epsilon = M/Re$ in the non-dimensional variables. $v = (\rho, u_1, u_2, u_3, p)^{\mathrm{T}}$ are the primitive variables. Using the parabolic symmetrizer derived in [24], the following non-dimensional variables are obtained, $\tilde{w}^{\mathrm{T}} = \left(\frac{a}{\sqrt{\gamma}\rho\tilde{\rho}}, \tilde{u}_1, \tilde{u}_2, \tilde{u}_3, -\frac{a}{\sqrt{\gamma(\gamma-1)}}\frac{\tilde{\rho}}{\rho} + \sqrt{\frac{\gamma}{\gamma-1}}\frac{1}{\rho a}\tilde{p}\right)$.

To simplify the notation, we show this in a Cartesian setting. But we stress that the analysis holds in the curvilinear case as well (see [6] for a derivation of the equations in a curvilinear system). The proposed boundary condition (on the left boundary) in the symmetrized system is

$$\alpha\widehat{A}_1^{+}\tilde{w} - \epsilon\widehat{F}_w^{V} = g,$$

where $g = (g_1, g_2, g_3, g_4, g_5)^{\mathrm{T}}$. (On the right boundary $\widehat{A}_1^{+}$ would be replaced by $\widehat{A}_1^{-}$.) In the symmetrized system we have $\widehat{F}_w^{V} = (0, F_2^{V}, F_3^{V}, F_4^{V}, F_5^{V})^{\mathrm{T}}$. Since we are considering the Cartesian case, we have $\widehat{A}_1 = A_1$ and $\widehat{F}_w^{V} = F_w^{V}$. The eigenvectors of A_1 are found as columns in,

$$X = \begin{pmatrix} 0 & 0 & -\sqrt{\frac{\gamma-1}{\gamma}} & \frac{1}{\sqrt{2\gamma}} & \frac{1}{\sqrt{2\gamma}} \\ 0 & 0 & 0 & \frac{1}{\sqrt{2}} & -\frac{1}{\sqrt{2}} \\ 1 & 0 & 0 & 0 & 0 \\ 0 & 1 & 0 & 0 & 0 \\ 0 & 0 & \frac{1}{\sqrt{\gamma}} & \sqrt{\frac{\gamma-1}{2\gamma}} & \sqrt{\frac{\gamma-1}{2\gamma}} \end{pmatrix},$$

such that $X^{\mathrm{T}}A_1X = \Lambda_1 = \mathrm{diag}(u_1, u_1, u_1, u_1 + a, u_1 - a)$. We begin by considering the case $\alpha = 1$.

For a subsonic inflow ($a > u_1 > 0$) the first four eigenvalues of Λ_1 are positive. If we diagonalize the boundary condition we obtain $\Lambda_1^+ c - \epsilon X^{\mathrm{T}} F_w^V = X^{\mathrm{T}} g = g^c$. It can easily be shown that the five conditions are linearly independent.

The case of subsonic outflow ($0 > u_1 > -a$) is more difficult. We start by studying the proposed boundary condition, $A_1^+ u - \epsilon F_w^V = g$, in the symmetric system. Again, we apply the transformation to diagonal form,

$$\begin{aligned}
&-\epsilon F_3^V = g_3,\\
&-\epsilon F_4^V = g_4,\\
&-\epsilon F_5^V = -\sqrt{\gamma-1}g_1 + g_5,\\
&(u_1+a)\left(\tilde{u}_1 + \sqrt{\gamma}\tilde{u}_2 + \sqrt{\gamma-1}\tilde{u}_5\right) - \epsilon\left(\sqrt{\gamma}F_2^V + \sqrt{\gamma-1}F_5^V\right) = \left(g_1 + \sqrt{\gamma}g_2 + \sqrt{\gamma-1}g_5^I\right),\\
&-\epsilon\left(-\sqrt{\gamma}F_2^V + \sqrt{\gamma-1}F_5^V\right) = \left(g_1 - \sqrt{\gamma}g_2 + \sqrt{\gamma-1}g_5\right).
\end{aligned} \tag{28}$$

In this case, we should have four boundary conditions. The first two equations are independent of the last three as before. However, the last three equations are linearly independent and the proposed set of boundary conditions overspecify the partial differential equation. One remedy is simply to remove the fifth condition and prove that the solution is bounded anyway. This approach is taken in [3].

We want to keep the structure of the boundary conditions and hence we will derive a new fifth condition based on the third and fourth. (One way or another the linear dependence has to be expressed in the scheme.) We change the notation for all the boundary conditions by introducing new variables and expressions on the data: $\sum_{j=1}^5 (X^{\mathrm{T}})_{ij}(F_w^V) = G_i$; $\sum_{j=1}^5 (X^{\mathrm{T}})_{ij}(c) = c_i$ and $\sum_{j=1}^5 (X^{\mathrm{T}})_{ij}(g) = g_i^C$. We propose the well-posed set of boundary conditions,

$$\begin{aligned}
&-\epsilon G_1 = g_1^C,\\
&-\epsilon G_2 = g_2^C,\\
&-\epsilon G_3 = g_3^C,\\
&(u_1+a)c_4 - \epsilon G_4 = g_4^C.
\end{aligned}$$

We note that $-G_4 + 2\sqrt{\gamma-1}G_3 = G_5$. Hence, the following condition merely constitutes a linear combination of the first four:

$$-(u_1+a)\tilde{c}_4 - \epsilon G_5 = -g_4^C + 2\sqrt{\gamma-1}g_3^C = g_5^C. \tag{29}$$

The last equality serves as a definition. This relation is added as a fifth equation to complete the form of the boundary conditions. The factor $-(u_1+a)$ is put in a 5 by 5 matrix in the 5,4 position, which is then transformed back to the symmetric system to form a matrix A'. This can readily be done in a code and we do not derive the exact form of A'.

Remark. Note that the data in the characteristic system is compatible by construction, i.e. g_5^C is given by $g_1^C, \ldots, g_4^C$. However, it may not be as obvious that data are still compatible if the outflow condition is specified as

$$(A^+ + A')(u - g^I) - \epsilon(F^V - g^V) = 0, \tag{30}$$

where the $g_1^V = F_1^V = 0$. But since both variables and data are subject to the same linear operations (that is a multiplication by X^{T}), it is clear that they will be compatible.

Remark. In the construction of the penalty terms, we split the treatment into an inviscid and a viscous part and choose appropriate data for each part. We stress that this is for convenient programming and that the boundary conditions actually imposed are precisely the ones given above. The effect of the penalty terms will *not* force the solution to satisfy the inviscid data *and* the viscous data, but their sum. In practice we choose data for g^I and g^V separately in all positions. The boundary treatment will automatically pull out the relevant part of the data and enforce the correct boundary conditions as shown above.

Finally, we need to show for well-posedness that the proposed boundary conditions bound the solution. The boundary terms appearing in the energy estimate at $x = 0$ (the left boundary) is

$$0 = \|\tilde{w}\|_t^2 - \int_{x=0} c^{\mathrm{T}}(\Lambda_1 c - 2\epsilon X^{\mathrm{T}} F^V)\,\mathrm{d}y\,\mathrm{d}z = \|\tilde{w}\|_t^2 - \int_{x=0} \sum_{i=1}^{5} \frac{1}{\lambda_i}((\lambda_i c_i - \epsilon G_i^V)^2 - (\epsilon G_i^V)^2)\,\mathrm{d}x\,\mathrm{d}z. \tag{31}$$

The negative boundary terms need to be supplied with boundary conditions. For $i = 1, 2, 3$, $\lambda_i = u_1 < 0$, the viscous flux is specified bounding correct terms. For $i = 4$, we impose $\lambda_4 c_4 - \epsilon G_4^V = 0$ (if homogeneous boundary data are assumed). With those boundary conditions (31) becomes

$$\|\tilde{w}\|_t^2 - \int_{x=0} \left(\sum_{i=1}^{3} \left(\frac{1}{\lambda_i}(\lambda_i c_i - \epsilon G_i^V)^2 \right) + \frac{1}{\lambda_5}(\lambda_5 c_5 - \epsilon G_5^V)^2 - \frac{1}{\lambda_4}(\epsilon G_4^V)^2 - \frac{1}{\lambda_5}(\epsilon G_5^V)^2 \right) \mathrm{d}x\,\mathrm{d}z. \tag{32}$$

The only term in (32) that may have the wrong sign is $\frac{(\epsilon G_5^V)^2}{\lambda_5}$. We can use the bounded term $\frac{1}{\lambda_4}(\epsilon G_4^V)^2$ to help. With $\lambda_4 = u_1 + a > 0$ and $\lambda_5 = u_1 - a$ and using the last condition (29), i.e. $-\lambda_4 c_4 + \epsilon G_5^V = 0$, we may write

$$\begin{aligned} \frac{1}{\lambda_4}(\epsilon G_4^V)^2 + \frac{1}{\lambda_5}(\epsilon G_5^V)^2 &= \frac{1}{u_1 + a}(-(u_1 + a)c_4)^2 + \frac{1}{u_1 - a}((u_1 + a)c_4)^2 = (u_1 + a)^2 c_4^2 \left(\frac{u_1 + a + u_1 + a}{(u_1 - a)(u_1 + a)}\right) \\ &= (u_1 + a)^2 c_4^2 \left(\frac{2u_1}{u_1^2 - a^2}\right) > 0. \end{aligned}$$

The last inequality is due to $u_1 < 0$ (subsonic outflow at the left boundary $x = 0$). Since the term is positive we have a bound on the solution.

Remark. We assumed that $\alpha = 1$ in the boundary conditions. But it is obvious that the linear dependence introduced is valid for any α as long as α multiplies both A^+ and A'.

Appendix B. Well-posedness specifying pressure and viscous fluxes

For simplicity we consider the Navier–Stokes equations on the unit cube in Cartesian form. We will study a subsonic outflow at $x = 0$ and assume that all other boundaries do not contribute to a growth of the solution. As before, we want the boundary conditions to take the form,

$$\alpha(A^+ + A')w - \epsilon \widehat{F}^V = g^w.$$

Instead of using the ingoing characteristic we will now use the pressure, which will determine the form of A'. We transform the boundary condition to diagonal form by multiplying from left with X^{T} defined in Appendix A,

$$\alpha(\Lambda^+ + \Lambda')c - \epsilon \widehat{G}^V = g^C,$$

where

$$c = \left(\tilde{u}_3, \tilde{u}_4, -\frac{\sqrt{\gamma}a}{\sqrt{\gamma - 1}\rho}\tilde{\rho}, \sqrt{\gamma}\tilde{u}_1 + \frac{\sqrt{\gamma}}{\rho a}\tilde{p}, -\sqrt{\gamma}\tilde{u}_1 + \frac{\sqrt{\gamma}}{\rho a}\tilde{p} \right)^{\mathrm{T}}. \tag{33}$$

The energy equation before application of boundary conditions has the form

$$\|w\|_t^2 \leqslant \int_{x=0} c^{\mathrm{T}}(\Lambda^- + \Lambda^+)c - 2\epsilon c^{\mathrm{T}} \widehat{G}^V\,\mathrm{d}y\,\mathrm{d}z. \tag{34}$$

In this case $u_1 < 0$ and $\Lambda^+ = \mathrm{diag}(0, 0, 0, u + a, 0)$. If we want pressure to be the variable appearing in the boundary condition we note that

$$c_4 + c_5 = \frac{2\sqrt{\gamma}}{\rho a}\tilde{p}. \tag{35}$$

Hence, we propose the following four boundary conditions on component form,

$$-\epsilon G_1 = g_1^C, \tag{36}$$
$$-\epsilon G_2 = g_2^C, \tag{37}$$
$$-\epsilon G_3 = g_3^C, \tag{38}$$
$$\alpha\lambda_4(c_4 + c_5) - \epsilon G_4 = g_4^C. \tag{39}$$

We use these four conditions to derive a fifth as a linear combination,

$$-\alpha\lambda_4(c_4 + c_5) - \epsilon G_5 = -g_4^C + 2\sqrt{\gamma - 1}g_3^C. \tag{40}$$

The next step is to show that this set bounds the energy (34). Write the energy in component form,

$$\begin{aligned}\|w\|_t^2 &\leqslant \int_{x=0} \lambda_1 c_1^2 + \lambda_2 c_2^2 + \lambda_3 c_3^2 + \lambda_4 c_4^2 + \lambda_5 c_5^2 - 2\epsilon(c_1 G_1 + c_2 G_2 + c_3 G_3 + c_4 G_4 + c_5 G_5)\,\mathrm{d}y\,\mathrm{d}z \\ &\leqslant \int_{x=0} \lambda_4 c_4^2 + \lambda_5 c_5^2 - 2\epsilon(c_1 G_1 + c_2 G_2 + c_3 G_3 + c_4 G_4 + c_5 G_5)\,\mathrm{d}y\,\mathrm{d}z.\end{aligned} \tag{41}$$

Using (36)–(38), assuming homogenous data and omitting the bounded terms yields

$$\|w\|_t^2 \leqslant \int_{x=0} \lambda_4 c_4^2 + \lambda_5 c_5^2 - 2\epsilon(c_4 G_4 + c_5 G_5)\,\mathrm{d}y\,\mathrm{d}z.$$

Inserting (39) and (40) yields

$$\begin{aligned}\|w\|_t^2 &\leqslant \int_{x=0} \lambda_4 c_4^2 + \lambda_5 c_5^2 - 2\alpha(c_4\lambda_4(c_4 + c_5) - c_5\lambda_4(c_4 + c_5))\,\mathrm{d}y\,\mathrm{d}z \\ &= \int_{x=0} \lambda_4 c_4^2 + \lambda_5 c_5^2 - 2\alpha(c_4^2\lambda_4 - c_5^2\lambda_4)\,\mathrm{d}y\,\mathrm{d}z = \int_{x=0} (1 - 2\alpha)\lambda_4 c_4^2 + (1 + 2\alpha)\lambda_5 c_5^2\,\mathrm{d}y\,\mathrm{d}z < 0.\end{aligned} \tag{42}$$

The last inequality holds if $\alpha > 1/2$. Note that this is the same condition as in the characteristic case. We conclude that at $x = 0$,

$$\Lambda' = \begin{pmatrix} 0 & 0 & 0 & 0 & 0 \\ 0 & 0 & 0 & 0 & 0 \\ 0 & 0 & 0 & 0 & 0 \\ 0 & 0 & 0 & 0 & \lambda_4 \\ 0 & 0 & 0 & -\lambda_4 & -\lambda_4 \end{pmatrix}. \tag{43}$$

Remark. On a general boundary Λ' will take exactly the same form with the difference that the eigenvalues are based on the normal velocity.

References

[1] Heinz-Otto Kreiss, Joseph Oliger, Comparison of accurate methods for the integration of hyperbolic equations, Tellus XXIV 3 (1972).
[2] Jan Nordström, Magnus Svärd, Well posed boundary conditions for the Navier–Stokes equations, SIAM J. Numer. Anal. 43 (3) (2005) 1231–1255.
[3] Jan Nordström, The use of characteristic boundary conditions for the Navier–Stokes equations, Comput. Fluids 24 (5) (1995) 609–623.
[4] Heinz-Otto Kreiss, Jens Lorenz, Initial Boundary Value Problems and the Navier–Stokes Equations, Academic Press, New York, 1989.
[5] B. Gustafsson, A. Sundström, Incompletely parabolic systems in fluid dynamics, SIAM J. Appl. Math. (1978).
[6] John C. Strikwerda, Initial boundary value problems for incompletely parabolic systems, Commun. Pure Appl. Math. 9 (3) (1977) 797–822.
[7] P.D. Lax, R.D. Richtmyer, Survey of the stability of linear finite difference equations, Commun. Pure Appl. Math. IX (1956).

[8] G. Strang, Accurate partial difference methods II. Non-linear problems, Num. Math. 6 (1964) 37–46.
[9] J.S. Hesthaven, D. Gottlieb, A stable penalty method for the compressible Navier–Stokes equations: I open boundary conditions, SIAM J. Sci. Comput. (1996).
[10] M.H. Carpenter, J. Nordström, D. Gottlieb, A stable and conservative interface treatment of arbitrary spatial accuracy, J. Comput. Phys. 148 (1999).
[11] H.-O. Kreiss, G. Scherer, Finite element and finite difference methods for hyperbolic partial differential equations, Mathematical Aspects of Finite Elements in Partial Differential Equations, Academic Press, Inc., 1974.
[12] H.-O. Kreiss, G. Scherer, On the existence of energy estimates for difference approximations for hyperbolic systems. Technical Report, Department of Scientific Computing, Uppsala University, 1977.
[13] Bo Strand, Summation by parts for finite difference approximations for d/dx, J. Comput. Phys. 110 (1994).
[14] M.H. Carpenter, D. Gottlieb, S. Abarbanel, Time-stable boundary conditions for finite-difference schemes solving hyperbolic systems: methodology and application to high-order compact schemes, J. Comput. Phys. 111 (2) (1994).
[15] J. Nordström, M.H. Carpenter, Boundary and interface conditions for high-order finite-difference methods applied to the Euler and Navier–Stokes equations, J. Comput. Phys. 148 (1999).
[16] J. Nordström, M.H. Carpenter, High-order finite difference methods, multidimensional linear problems, and curvilinear coordinates, J. Comput. Phys. 173 (2001).
[17] K. Mattsson, M. Svärd, J. Nordström, M.H. Carpenter, Accuracy Requirements for Transient Aerodynamics. AIAA Paper 2003-3689, 2003.
[18] Ken Mattsson, Jan Nordström, Summation by parts operators for finite difference approximations of second derivatives, J. Comput. Phys. 199 (2) (2004).
[19] Magnus Svärd, On coordinate transformation for summation-by-parts operators, J. Sci. Comput. 20 (1) (2004).
[20] Ken Mattsson, Magnus Svärd, Jan Nordström, Stable and accurate artificial dissipation, J. Sci. Comput. 21 (1) (2004) 57–79.
[21] Magnus Svärd, Ken Mattsson, Jan Nordström, Steady state computations using summation-by-parts operators, J. Sci. Comput. 24 (1) (2005) 79–95.
[22] Magnus Svärd, Jan Nordström, On the order of accuracy for difference approximations of initial-boundary value problems, J. Comput. Phys. 218 (1) (2006) 333–352.
[23] B. Gustafsson, H.-O. Kreiss, J. Oliger, Time Dependent Problems and Difference Methods, John Wiley & Sons, Inc., 1995.
[24] Saul Abarbanel, David Gottlieb, Optimal time splitting for twoand three-dimensional Navier–Stokes equations with mixed derivatives, J. Comput. Phys. (1981).
[25] R.A. Horn, C.R. Johnson, Matrix Analysis, Cambridge University Press, 1990.
[26] T.H. Pulliam, D.S. Chaussee, A diagonal form of an implicit approximate-factorization algorithm, J. Comput. Phys 39 (1981) 347–363.
[27] B. Engquist, A. Majda, Radiation boundary conditions for acoustic and elastic wave calculations, Commun. Pure Appl. Math. 32 (1979) 313–357.